JOURNAL OF THERMOPHYSICS AND HEAT TRANSFER
Vol. 7, No. 2, April–June 1993

Simulation of Range-Resolved DIAL Measurements on In-Flight Rocket Plumes

C. T. Christou,* R. T. Loda,† and D. A. Levin*
Institute for Defense Analyses, Alexandria, Virginia 22311

Feasibility studies were carried out for a ground-based experiment using the differential absorption LIDAR (DIAL) method, to measure spatially resolved rocket plume temperature profiles from solid-aluminized propellants. The core of this effort was a numerical simulation of the dynamics of the laser-plume interaction and the retrieval of average temperatures from the received signals using parameters appropriate to a low-altitude rocket plume. Signal-to-noise ratios were adequate for the assumed experimental conditions and for both a clear and moderately clear atmosphere, to ensure detectability of the returned signals over most of the plume. For the chosen laser frequencies, the simulated experimental results indicate reasonable quantitative agreement with flowfield model predictions.

Introduction

A DETAILED analysis was conducted to assess the feasibility of a ground-based DIAL experiment which would measure spatially resolved airborne rocket plume temperature profiles. To date, plume temperature profile data do not exist despite the large number of flowfield predictions. The interaction between the plume intrinsic core and the ambient atmosphere cannot be simulated in laboratory or chamber measurements. Thus, the possibility of measuring temperatures of in-flight rocket plumes with a remote sensing technique is being considered. HD (hydrogen-deuterium) Raman shifted Nd:Glass lasers would be used to provide tunable radiation over the 5660–5910 cm^{-1} region of the spectrum, which coincides with the R-branch of the 0-2 ro-vibronic band of HCl, a major constituent of solid rocket motor (SRM) plumes.

To implement the DIAL technique, two laser pulses are sent out over the same path. One is tuned to the frequency of an absorption line of the gaseous species of interest and the other is tuned off-resonance. The difference in the intensity backscattered by solid plume particulates can then be related to the absorption coefficient of a resonant gaseous species such as HCl. If the measurement is repeated for a second absorption line of the same species, the rotational-vibrational temperature may be extracted from the values of the two absorption coefficients, assuming the gas is in thermal equilibrium. The DIAL technique has been successful in atmospheric applications, but has not yet been tested in a plume environment where physical parameters vary much more rapidly, spatially as well as temporally.

There are complications which can arise in the DIAL experiment which would produce an erroneous temperature measurement. A specific species is selected as the interrogated molecular system based on its relatively high abundance in the plume and the availability of well-characterized absorption spectra. The HCl molecular system satisfies both of these requirements; however, due to the near equality of plume water and HCl mole fractions, the location of absorption lines of water must also be determined in order to avoid potential interference. The high temperature absorption lines of a simple polyatomic system such as water are difficult to calculate and have undergone limited experimental study at temperatures as high as 2000 K. A second complication is absorption of the laser radiation by ambient atmospheric species. These issues have been carefully analyzed in Ref. 1 to produce an optimal set of usable HCl transitions. The $P(4, 6, 9, 10, 11, 14, 16, 18)$ lines were found to have less than 90% transmission through the atmosphere. Of the possible rotational transitions for the R-branch, the $R(1, 3, 6, 7, 10)$ lines were found to be free of either hot water interference or atmospheric attenuation.[1] Therefore, they could be considered as potential laser interrogation wavelengths. The final choice of on-resonance laser frequencies for this simulation corresponds to the $R(6)$ and $R(7)$ lines for reasons which will be discussed below. Another issue of concern is that of the effect of Doppler frequency shifts due to the moving masses in the plume. This factor, as well as the finite laser width, have so far been considered in an approximate fashion. Preliminary results indicate that for the particular relative geometry of plume and laser beam considered in this study, these effects will not pose a serious problem.

The purpose of this article is to report the detailed numerical simulation of a future DIAL-plume measurement. The proposed experiment is sufficiently complex and so costly that the use of preflight numerical simulation techniques is crucial to assess feasibility concerns.

This simulation effort focused on determining the probability of the extraction of an average temperature which will realistically represent the interrogated region of the plume. Reasons for concern were the large temperature gradients relative to the proposed range resolution, as well as the nonlinear relationship between the average absorption coefficient and the average temperature in a range cell. The modeling is divided into two parts, the "forward" and "inverse" calculations. The forward problem consists of the computation of the returned laser power from the radial range cells at a particular axial plume location. The inverse problem involves the estimation of a range-resolved average temperature from the extracted values of the absorption coefficients and known line parameters. We began by examining a 40-km-alt flowfield solution for a representative rocket, obtained from the standard plume flowfield model SPF2.[2] The numerical simulation employed here is sufficiently general to apply to other plume flowfield predictions. Figures 1a (full plume) and 1b (area of Mach disk) show contour plots of the temperature variation as a function of axial distance from the nozzle (X) and radial distance from the axis (Y). If the proposed range resolution of 3.15 m is superimposed on these figures it can be seen that it is large relative to the spatial temperature variation through-

Presented as Paper 91-0461 at the AIAA 29th Aerospace Sciences Meeting, Reno, NV, Jan. 7–10, 1991; received Sept. 19, 1991; revision received March 23, 1992; accepted for publication March 24, 1992.

*Research Staff Member, Science and Technology Division. Member AIAA.
†Research Staff Member, Science and Technology Division.

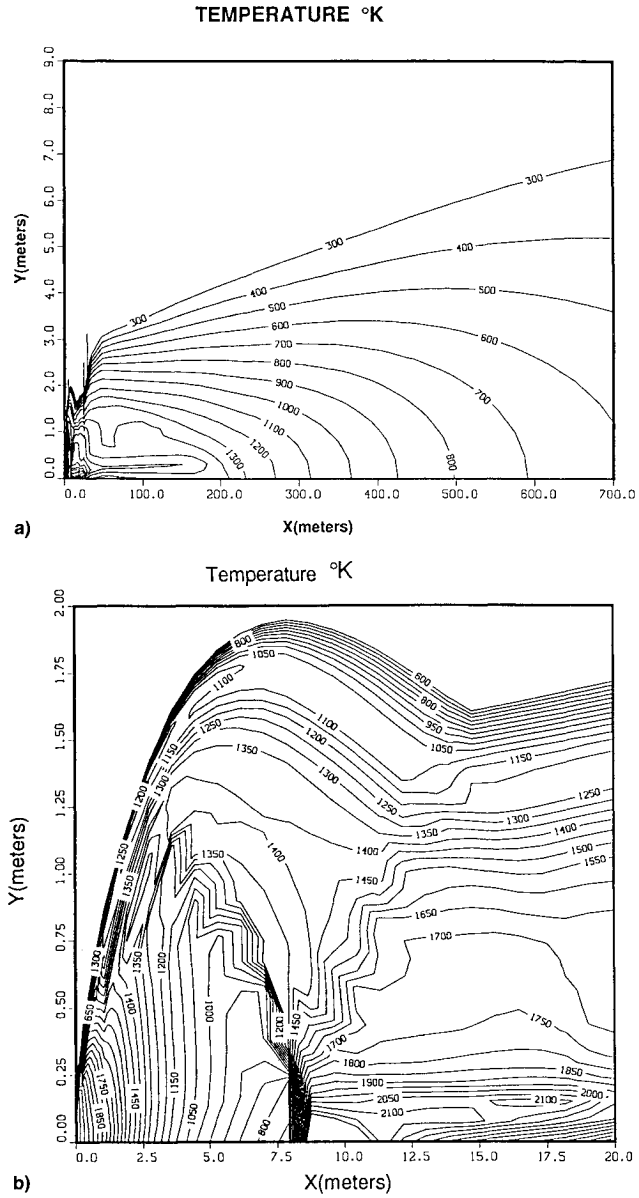

Fig. 1 a) Temperature contours for a solid propellant at 40-km altitude, and b) is the expanded view. The rocket nozzle is located at the origin of the graph.

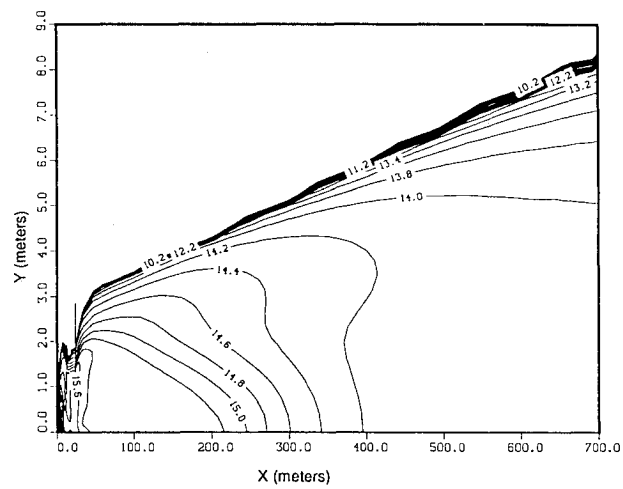

Fig. 2 Concentration of HCl for a solid propellant at 40-km altitude, contour levels in Abs[$\log_{10}$(molecules/cm^3)]. The rocket nozzle is located at the origin of the graph.

out the plume. The DIAL measurement will therefore represent an average over the range cell. Figure 2 is a plot of the HCl concentration. The SPF2 model run used in these calculations uses a distribution of Al_2O_3 particles of three different radii, 1.52, 2.83, and 5.26 μ.

LIDAR Equation and Definitions

The analysis of the DIAL experiment is based on the generalized light detection and ranging (LIDAR) equation,[3] which we used to model the transmission and backscattering of laser radiation through the plume

$$P_r(\nu_r, R) = P_0(\nu_0)KT(\nu_0)T(\nu_r)Y(R)\Delta R\beta(\nu_0, \theta)A_r/R^2 \quad (1)$$

where

ν_0, ν_r	=	transmitted and received frequencies ($\nu_0 = \nu_r$ for elastic scattering)
R	=	distance from scattering element to detector (range)
$P_r(\nu_r, R)$	=	received power
$P_0(\nu_0)$	=	transmitted power of the laser pulse
K	=	efficiency of total optical system
$T(\nu_0)$, $T(\nu_r)$	=	one way transmittances at the transmitted and received frequencies
A_r	=	effective receiver aperture
$\beta(\nu_0, \theta)$	=	volume coefficient
$Y(R)$	=	geometrical factor to account for the overlap of transmitted and received fields of view and equal to 1 for total overlap
ΔR	=	$c\tau/2 = c(\tau_p + \tau_s + \tau_c)/2$ = range resolution of measurement
c	=	speed of light (3×10^{10} cm/s)
τ_p	=	laser pulse length
τ_s	=	species optical interaction time
τ_c	=	detection system response time

The total transmittance $T(\nu)$ can be expressed as

$$T(\nu) = \exp\left[-\int_0^R \alpha(\nu, r)\, dr\right] \quad (2)$$

where

$$\alpha(\nu, r) = \alpha_A(\nu, r) + \alpha_G(\nu, r) + \alpha_P(\nu, r) \quad (3)$$

is the total extinction coefficient due to absorption and scattering arising from atmospheric species (A), plume particulates (P), and the species of interest (G). The atmospheric extinction coefficient α_A was evaluated for the two limiting cases of a clear atmosphere containing only gaseous molecules and no pollutants [Eq. (4a)] and one with aerosols [Eq. (4b)][3,4]:

$$\sigma_R = 4.56[\lambda(\mu)/0.55]^{-4} \times 10^{-27}\ \text{cm}^2$$

$$N_G = 2.55 \times 10^{19}/\text{cm}^3 \quad (4a)$$

$$\alpha = (3.91/V_m)[0.55/\lambda(\mu)]^q, \quad q = 1.3,\ V_m = 16\ \text{km} \quad (4b)$$

We obtained signal levels for a "moderately clear" atmosphere by interpolation between the transmission factors given by Eqs. (4a) and (4b).

The values of E_0 (300 mJ/pulse), τ_p (10 ns), τ_c (10 ns), K (0.1), A_r (5000 cm^2) were chosen in accordance with the specifications of the instrumentation to be developed for the DIAL experiment, which yields a value of 3.15 m for ΔR. The interaction time was set equal to 1 ns, although it is essentially instantaneous.

The detection of a returned signal presupposes scattering of the radiation by larger sized particles in the plume. In general, the plumes of solid propellant rockets contain Al_2O_3 in the form of solid particulates whose radius can vary between

0.01–20 μ with a mean ~1–2 μ.[5-7] The interaction of these particles with radiation obtainable from a Raman shifted Nd:Glass laser ($\lambda \simeq 1.7$ μ) must then be described by the Mie scattering theory.[8] The physics of the scattering mechanism is contained in the volume backscattering coefficient β, which depends on the size distribution of Al_2O_3 particles and is given by the integral

$$\beta(\nu, \theta) = N_P \int_{a_{\min}}^{a_{\max}} f(a) \frac{d\sigma}{d\Omega}(\nu, \theta, a)\, da \qquad (5)$$

where N_p is the number density of scattering particles, $f(a)$ da is the fraction of the total number of particles with radius between a and $a + da$, and $d\sigma/d\Omega(\nu, \theta, a)$ is the differential scattering cross section at frequency ν and scattering angle θ.[4] Since the DIAL experiment will involve a monostatic arrangement (colocated transmitter and detector), the scattering angle θ will always equal 180 deg. The index of refraction was obtained from an SPF2-SIRRM file.[5-7,9] For simplicity, we assumed spherical particles which can be treated exactly by Mie theory and single (as opposed to multiple) scattering which is valid for the plume predicted by SPF2 to be optically thin.

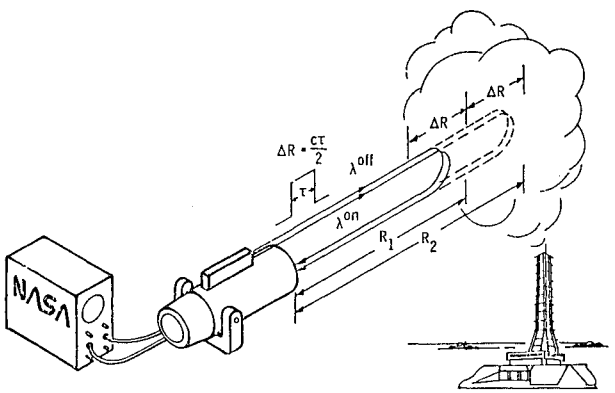

Fig. 3 Schematic of a two laser wavelength DIAL measurement applied to the detection of HCl in an SRM cloud.

DIAL Technique and Geometry

If it is assumed that the two wavelengths λ_{on} and λ_{off} are close enough together so that $\beta_{on} = \beta_{off}$, $\sigma_p(\lambda_{on}) = \sigma_p(\lambda_{off})$, it can be shown that

$$\bar{\alpha}\left(R_1 + \frac{\Delta R}{2}\right) = \frac{1}{2\Delta R} \ln\left[\frac{P_r^{off}(2)P_r^{on}(1)}{P_r^{on}(2)P_r^{off}(1)}\right] \qquad (6)$$

where $\bar{\alpha}[R_1 + (\Delta R/2)]$ is the average value of the HCl absorption coefficient in the range cell ΔR, R_1 is the penetration distance into the plume, and $R_2 = R_1 + \Delta R$. $P_r^{off}(1)$, $P_r^{on}(1)$ refer to power measurements at R_1, and $P_r^{off}(2)$, $P_r^{on}(2)$ refer to power measurements at R_2. By varying the position of range cell 2 with respect to the leading edge of the cloud, a spatial profile of the HCl absorption coefficient from the edge of the cloud to a penetration distance R_2 into the cloud can be obtained.[10] A schematic diagram of the DIAL technique is shown in Fig. 3.[10] The simplest geometry one could consider for the DIAL experiment is that in which the laser beam intersects the longitudinal plume axis at a 90-deg angle (Fig. 4).

Plume parameters were obtained from SPF2 and include temperatures, pressures, mole fractions of HCl, and the number densities of the Al_2O_3 particles corresponding to the three particle radii. The number and values of radial gridpoints (for the half-plume) is given for each axial location. The modeling program establishes the width of the plume and then divides it into segments of length ΔR (Fig. 4). Average values for β, α_p, and α_{HCl} are calculated in each bin from the values at

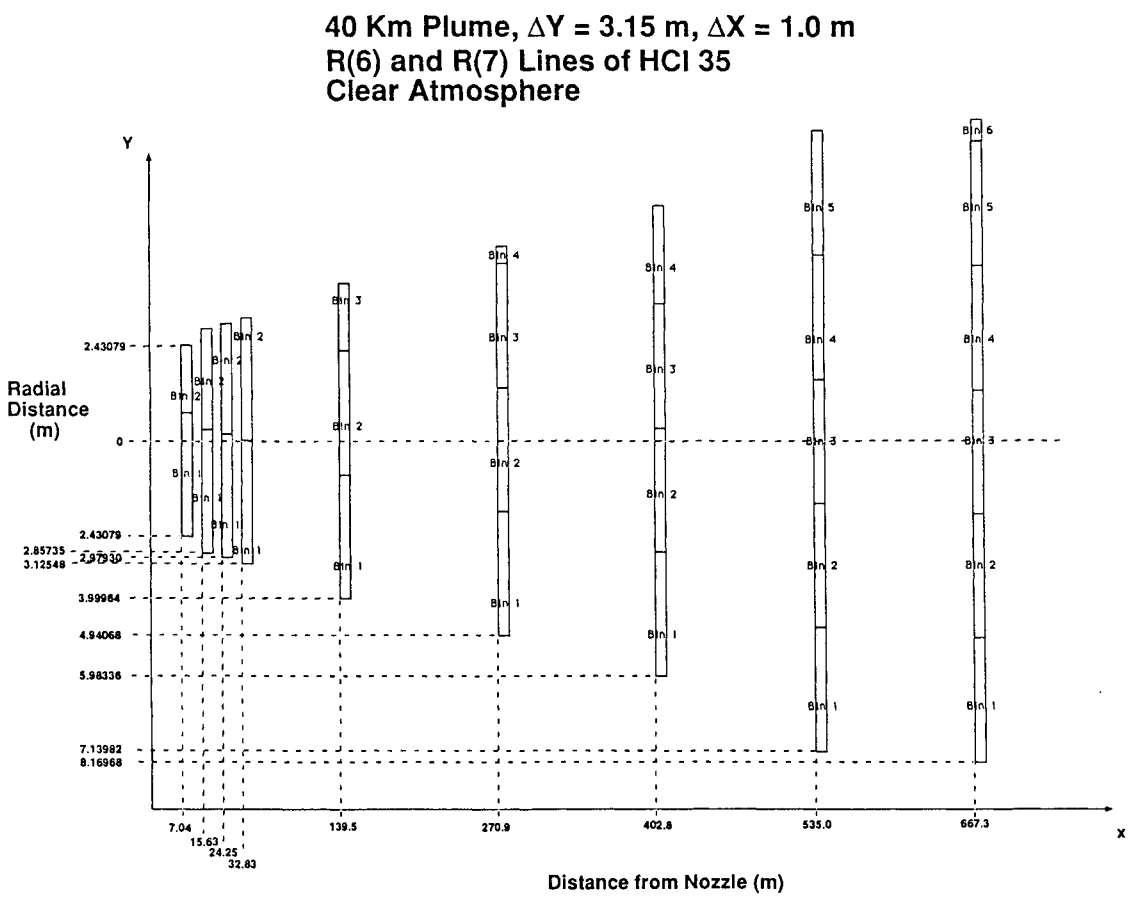

Fig. 4 Plume geometry and locations of range cells.

each gridpoint of β_i, α_{pi}, and the HCl concentration, N_{HCl}. This is, in turn, obtained from the value of the HCl mole fraction given by SPF2, and the ideal gas law. The absorption cross section $\sigma(\nu)$ for each of the two on-resonance frequencies is calculated from a subset of the high-resolution transmission molecular absorption (HITRAN) data base[11] using a procedure which will be discussed in the following section. All the relevant quantities are then combined into the LIDAR equation in order to compute the received power from each range cell ΔR, assuming a range of $R = 40$ km. In addition, the numerically averaged temperature T_{AVE}, as well as the temperature weighted by the HCl density $T_{AVE}(HCl)$, are computed in each range cell ΔR. Since HCl is the gas which will be used to extract values of temperature, it is valid to compare the DIAL results for T with $T_{AVE}(HCl)$. This constitutes the "forward" problem. We will now discuss the "inverse" problem.

Extraction of Temperature and Dependence on Line Shape

Spectral lines arising from molecular transitions between different energy states have a finite width which is caused by natural broadening, thermal motion of the molecules, as well as pressure effects. The exact width and shape of an HCl absorption line will depend primarily on the temperature and pressure in the corresponding region of the plume. One distinguishes among three most common broadening regimes:

1) Doppler broadening results from the random thermal motion of the molecules and determines the line shape at sufficiently low pressures and temperatures. For the extreme conditions of a plume, a quantitative criterion will be defined below. In the Doppler regime, theory predicts a Gaussian contour.

2) Pressure-broadened transitions are more dominant at higher pressures, as the name indicates. The spectral lineshape is Lorentzian.

3) At intermediate pressures, the spectral line shape is accurately represented by a Voigt profile, which is a convolution of Gaussian and Lorentzian line shapes. It may be expressed in terms of the real part of the error function of complex argument $w(z)$.[3,12]

Information regarding the HCl R-branch spectral lines, as well as the water lines, is contained in a data file extracted from the HITRAN data base.[11] In our modeling program we calculate the most general (Voigt) line shape centered about the input laser frequency which we chose to coincide with the centerline or resonant frequency. In order to establish the appropriate pressure-temperature regime at each gridpoint the following criterion was used. For a spectral transition with a Doppler width γ_D and a Lorentz width γ_L we define a Voigt parameter ζ

$$\zeta = \gamma_L/(\gamma_L + \gamma_D) \tag{7}$$

The Doppler and pressure-broadening regimes are defined as follows[13]:

$\gamma_L \ll \gamma_D$	$\zeta \to 0$	(Doppler limit)
$0.0 \le \zeta \le 0.5$		(Doppler regime)
$\gamma_L \gg \gamma_D$	$\zeta \to 1$	(Pressure limit)
$0.5 \le \zeta \le 1.0$		(Pressure regime)

Thus, in the limit of low ζ the Voigt profile should degenerate into a Gaussian contour, and in the limit of high ζ it should degenerate into a Lorentzian contour.

Knowledge of the shape of a transition line is critical when attempting to extract a temperature from DIAL measurements. It can be shown that the absorption coefficient is given by[12]

$$\alpha(\nu) = \frac{A_{ij}N(J' + J'' + 1)}{8\pi c\nu_{ij}^2 Q_r Q_v} f(\nu)\exp\left[\frac{-E(J'')}{kT}\right] SE(T) \tag{8}$$

where

A_{ij} = Einstein transition probability from ith (lower level) to jth (upper) level
ν_{ij} = frequency of ijth transition
Q_r = rotational partition function (constant at a given temperature)
Q_v = vibrational partition function (constant at a given temperature)
J' = rotational quantum number of the jth (upper) level of the transition
J'' = rotational quantum number of the ith (lower) level of the transition
$E(J'')$ = rotation energy of the lower level

$[1 - \exp(hc\nu_{ij}/kT)] = SE(T)$ = stimulated emission factor. The exponential represents a Boltzmann factor and $f(\nu)$ is a factor dependent on the line shape. The DIAL technique is based on the measurement of the absorption coefficients for two separate resonance lines of the 0–2 vibrational overtone of HCl, $\alpha_1(\nu_1)$, $\alpha_2(\nu_2)$. Subtraction of the linearized equation [obtained by taking the logarithm of both sides of Eq. (8)] for $\alpha_2(\nu_2)$ from the corresponding expression for $\alpha_1(\nu_1)$ yields

$$\ell n\left[\frac{\alpha_1(\nu_1)\nu_1^2 f_2(\nu_2)A_2(J' + J'' + 1)_2}{\alpha_2(\nu)\nu_2^2 f_1(\nu_1)A_1(J' + J'' + 1)_1}\right] = \frac{(E_2 - E_1)}{kT} \tag{9}$$

which gives the temperature in terms of the parameters of the two resonance lines. The importance of including the correct line shape factors f_2, f_1 becomes clear from Eq. (9). Without a priori knowledge of the line shape appropriate to the temperature-pressure conditions of the plume region under interrogation, the factor f_2/f_1 is unknown. On the other hand, from numerical examples we found that substitution of an erroneous line shape factor can lead to very large errors in the extracted temperature. In order to resolve this issue, we explored the various pressure-temperature regimes of our 40-km representative rocket plume. Applying the ζ criterion we found that practically the entire plume can be considered a Doppler regime. This is primarily a consequence of the low pressures ($P < 0.1$ atm) prevalent in the plume. In this case, the ratio of line shape factors does not involve the unknown temperature and pressure. The frequencies of the $R(6)$ and $R(7)$ lines are close enough together ($\nu_6 = 5779.549$ cm^{-1} and $\nu_7 = 5790.41$ cm^{-1}) to produce a ratio $f_2/f_1 = \nu_1/\nu_2 = 1.001879$ which is in turn close to unity. Therefore, for two laser integration wavelengths within 12 cm^{-1}, the omission of the line shape factor altogether would produce only a relatively small error in the temperature measurements.

Particle Size Distributions

We first chose the $R(1)$ ($\nu = 5706.094$ cm^{-1}) and the $R(7)$ ($\nu = 5790.41$ cm^{-1}) lines in our modeling. The off-resonance frequencies considered were 5789.05, 5791.00, and 5742.50 cm^{-1}. However, we found that the average values of $\beta_{on}(1)$, $\beta_{on}(7)$, and β_{off} differed considerably in each ΔR bin. Although $R(1)$ and $R(7)$ are separated by only 83 cm^{-1}, the values of $d\sigma/d\Omega$ obtained from the Mie theory vary sufficiently rapidly with the size parameter $2\pi a/\lambda$, that β differs greatly for the two wavelengths, especially for the larger size particles. As a result, the extracted values of $\bar{\alpha}$ were off by factors of up to 4, and the resulting temperature estimates by factors of 10 or 20!

We then decided to take two lines as close together as possible, $R(6)$ ($\nu = 5779.549$ cm^{-1}), $R(7)$, and an off-resonance frequency (5784.60 cm^{-1}) far enough away from a water line to avoid interference. We found that for the discrete size distribution of three radii used in SPF2, the average values of β were still not close enough in magnitude to extract a reasonable value of α. In actuality, a discrete Al_2O_3 particle size distribution in the plume is unphysical and an artifact of

SPF2 which can only handle discrete size distributions. For a continuous distribution the values of β would not vary as drastically with λ because the integration over the particle radius [Eq. (5)] would, in effect, smooth out the rapid variation.

The above analysis made us realize that to obtain physical results from our DIAL simulation, it would be necessary to fit a continuous distribution to the discrete one given by SPF2 gridpoint by gridpoint. To do this, we assumed a log-normal form

$$f(a) = \frac{1}{\mathscr{M}(10)\sqrt{2\pi}\sigma a} \exp\left[\frac{(\log a - \log a_1)^2}{2\sigma^2}\right] \quad (10)$$

where a_1 is the mode radius and σ is the standard deviation and proceeded to numerically fit this distribution to the discrete size particle densities given by SPF2.

The sensitivity analysis in the following section will make it clear why it is important that the values of β be virtually identical to extract a meaningful temperature profile.

Sensitivity Analysis and Estimate of Temperature Measurement Accuracy

The accuracy of the average temperature extracted through the DIAL technique as simulated in this article is based on two criteria: 1) the validity of Eq. (6) for a three interrogation wavelength scheme; and 2) the functional dependence of T on the absorption coefficient α [Eq. (9)] and the dependence, in turn, of α on the received laser power P_r [Eqs. (1) and (2)]. Both conditions are also dependent upon the HCl concentration within a spatial resolution bin ΔR.

Determination of conditions for which the first criteria is valid involves evaluations of functions e^{-x} and $\mathscr{M}x$ which are rapidly varying for $x < 1$. For the plume conditions predicted by SPF2 at 40 km, where the HCl density varies from $\sim 3 \times 10^{17}/\text{cm}^3$ near the nozzle to $\sim 1 \times 10^{14}/\text{cm}^3$ near the tail, $2\Delta R\bar{\alpha} \cong 0.007 << 1$, and therefore, a small error in the extracted value of $e^{-2\Delta R\bar{\alpha}}$ will produce a large error in $\bar{\alpha}$. The error in $\bar{\alpha}$ arises from the fact that the values of the backscattering coefficient β are not "exactly" the same for the off- and on-resonance frequencies, even when these differ by as little as six or seven wave numbers. For example, at station no. 90 (667-m downstream) we found that if we require a maximum error of 10% in the extracted temperature, then the ratio β_{on}/β_{off} must equal 0.9996 (α for station 90 is $\sim 3 \times 10^{-5}$ cm^{-1}).

Repeating the above calculation for a 20% error, we get $\beta_{on}/\beta_{off} = 0.9992$. Now, even theoretically, the values of α for the on- and off-resonant frequencies do not agree this well. At station no. 90, β_{on}/β_{off} varies between 0.9963–0.9974 (for the continuous size distribution). For the discrete size distribution given by SPF2, agreement is even worse (~0.954). The source of the difficulty is the low value of α ($\sim 3 \times 10^{-5}$ cm^{-1}) which arises from the correspondingly low HCl density in this region of the plume ($\sim 1.2 \times 10^{14}/\text{cm}^3$). If α were three orders of magnitude higher, say 3×10^{-2} cm^{-1}, then β_{on}/β_{off} for the same ΔR would only have to be as close as 0.6852. We got comparable results for station no. 10 (7 m) as well. This type of theoretical restriction allows little room for experimental error. Trying to get a better spatial resolution, i.e., decreasing ΔR, may not necessarily help. If the spatial resolution were $\Delta R = 157.5$ m, then a 10% error in temperature would require that $\beta_{on}/\beta_{off} = 0.998$, whereas a 20% error in T would require $\beta_{on}/\beta_{off} = 0.997$.

The second criteria for temperature accuracy is related to errors in measuring the three detected powers, $P_r^{off}(1)$, $P_r^{on}(1)$, and $P_r^{on}(2)$, which in turn introduces an error in T as given by Eqs. (6) and (9). We assume that there is no uncertainty related to the energy levels and that any laser error sources, such as a pulse to pulse power fluctuations or frequency stability, can be ignored. If the errors in measuring these terms are statistically independent, then the error in T, $\lambda(T)$ can be determined by

$$\lambda(T) = \left\{\left[\frac{\partial T}{\partial P_r^{on}(1)}\right]^2 \lambda^2[P_r^{on}(1)] + \left[\frac{\partial T}{\partial P_r^{on}(2)}\right]^2 \lambda^2[P_r^{on}(2)] + \left[\frac{\partial T}{\partial P_r^{off}(1)}\right]^2 \lambda^2[P_r^{off}(1)]\right\}^{1/2} \quad (11)$$

where terms such as $\lambda[P_r^{on,off}(1, 2)]$ represent the error in measured received power and are related to the signal-to-noise ratio (S/N) as

$$\lambda[P_r^{on,off}(1, 2)] = \frac{P_r^{on,off}(1, 2)}{(S/N)} \quad (12)$$

Application of Eq. (11) to Eqs. (6) and (9), with Eq. (12) substituted into that result, gives

$$\lambda(T) = \frac{kT^2}{(S/N)2\Delta R[E(J_2'') - E(J_1'')]}\left[\frac{1}{\bar{\alpha}_1^2} + \frac{1}{\bar{\alpha}_2^2} + \frac{(\bar{\alpha}_1 - \bar{\alpha}_2)^2}{\bar{\alpha}_1^2\bar{\alpha}_2^2}\right]^{1/2} \quad (13)$$

Equation (13) shows that the error in the temperature measurement is inversely proportional to the signal-to-noise ratio and the HCl concentration. The presence of the energy difference term in the denominator of Eq. (13) shows that if the β coefficients on and off resonance were equal then the error in the temperature measurement would be reduced as the wavelength difference increases. The wavelengths chosen for the simulation represent a compromise between these two conditions.

Results

The geometry of the plume relative to the direction of the laser beam assumed in this analysis is shown in Fig. 4. The laser beam enters the plume parallel to the vertical strips. These strips represent nine axial stations with range cells numbered in increasing order from the near-edge of the cloud. In order to account for the finite size of the field of view of the telescope ($\Delta X = 1$ m), the results for T_{AVE} were averaged over all neighboring axial points within 1 m of each axial station.

The first issue to be addressed is that of the detectability of the on- and off-resonance signals. In order for them to be discernible, will the difference between P_r^{on} and P_r^{off} be large enough relative to the detector sensitivity. To answer this question, we calculated the difference $P_r^{off} - P_r^{on}$ at the end of each range cell and divided by the noise-equivalent-power of the detector, equal in this case to 10^{-8} W. In this way, we get the difference in the signal-to-noise ratio, which we have plotted as a function of plume location in Fig. 5. For a clear and moderately clear atmosphere, the difference in signal-to-noise ratios were roughly equal for both the $R(6)$ and $R(7)$ lines and ranged from 2000 near the nozzle to 0.7 near the tail of the plume. Therefore, under these conditions the two signals appear to be discernible over the majority of the plume. In the presence of aerosols, however, the signal-to-noise ratio was reduced by two orders of magnitude. This implies that P_r^{off} and P_r^{on} would be clearly distinguishable over the whole width of the plume as far downstream as ~150 m. Any further down that that would result in the two signals being barely distinguishable only when close to the axis of the plume.

We also obtained plots of P_r^{on} and P_r^{off} for ranges near the plume. An example of these, corresponding to axial station no. 10, is shown in Fig. 6. The sudden increase in signal—a little before 40 km—signifies the near-edge of the plume and is due to the pronounced backscattering from the plume particles. The signal rises until particle extinction overtakes backscattering of the laser radiation. The sudden drop after 40 km signifies the far-edge of the plume. The upper curve represents P_r^{off}, while the lower curve represents P_r^{on}.

Results for the extracted average temperature in bin 1 are shown in Fig. 7 as a function of axial distance for nine axial

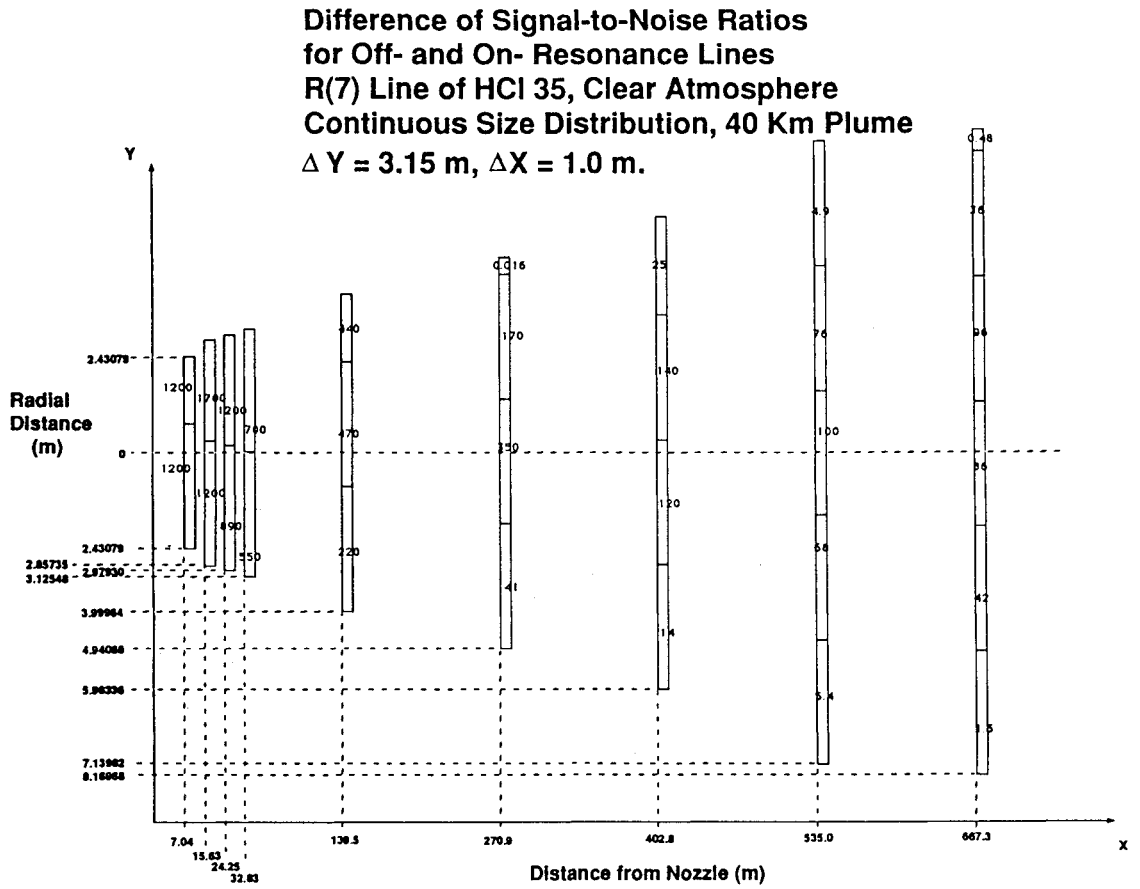

Fig. 5 Difference in signal-to-noise ratios from DIAL experiment stimulation.

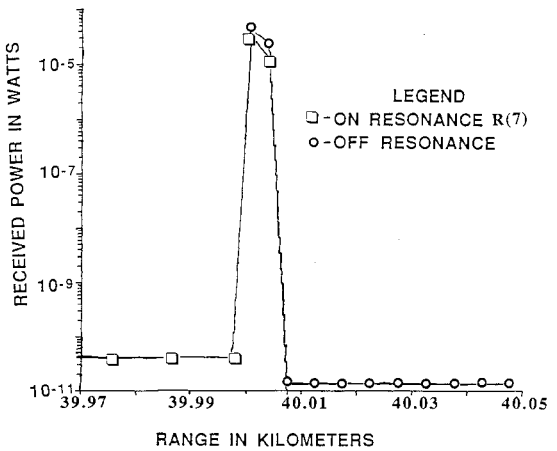

Fig. 6 LIDAR signal vs range at axial station no. 10 (7 m from the nozzle) for a clear atmosphere.

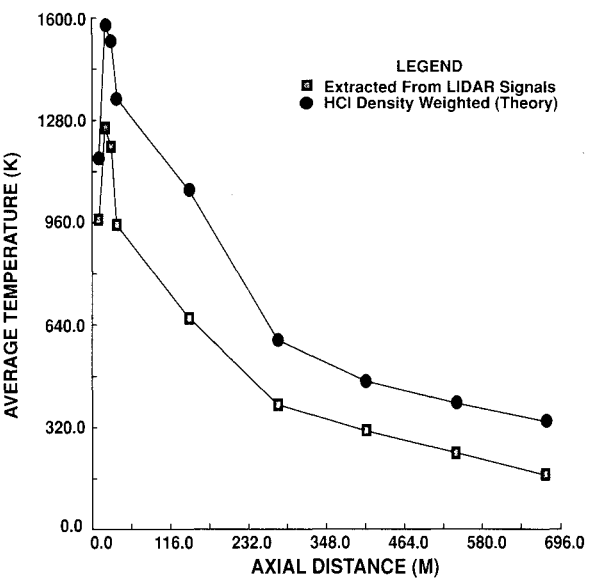

Fig. 7 Average temperatures from DIAL simulation, 40-km SPF2 plume, clear atmosphere, HCl $R(6)$, $R(7)$ lines, ΔX = 1.0 M, ΔY = 3.15 M, BIN = 1.

stations. These are compared to curves of T_{AVE} (HCl), the HCl density-weighted average temperature in each cell, obtained from the SPF2 flowfield prediction. Overall, the simulated DIAL curves exhibit the same structure as the theoretical SPF2 curves, except they tend to underpredict the average temperature. The similar shapes of these curves imply good qualitative agreement. An enlargement of the region of the Mach disk is shown in Fig. 8. Here again we notice a correspondence in shape and underlying structure between the two curves which suggests that the DIAL technique may help locate the region of the Mach disk. Examination of Figs. 7 and 8 show that the difference between the flowfield predicted temperature and the simulated experimentally obtained temperature is ~300 K. This value is consistent with Eq. (13) for the $R(6)$ and $R(7)$ lines, the cell averaged molecular absorption coefficients obtained, and the signal-to-noise ratios shown in Fig. 5. Alternatively, use of Eq. (13) shows that a signal-to-noise ratio of ~300 is required to obtain $\lambda(T) \sim \pm 200$ K. Figure 9 shows the regions of the plume where the expected error in the temperature would be less than 30% for a clear atmosphere based on the sensitivity analysis discussed above and Eq. (13).

Another issue is that of the Doppler frequency shifts generated by the moving masses in the plume. Gas and particle temperatures and velocities from SPF2 have been used to calculate the lineshift/linewidth ratios for selected portions of the representative rocket plume. The results for gaseous HCl are given in Fig. 10. Note that large lineshift/linewidth ratios

can occur, especially near the nozzle exit plane. The concern would be that these frequency shifts, if not accounted for, could produce intensity measurement errors which would translate into erroneous temperature estimates. Figure 11, however, shows the effect of the Doppler shift on the average absorption coefficient for a crossing geometry over the half-plume width depicted in Fig. 10. The 20-m axial station data gives lineshift/linewidth values of order 10%. However, the average absorption coefficient at the nonshifted line-center only changes by ~0.34%, which should not seriously affect the temperature measurement or the signal-to-noise ratio. At an axial location of 3.4 m, the average absorption coefficient at nonshifted line-center is lowered by 72%. This would alter the signal-to-noise ratio of the measurement. However, even this dramatic change in intensity should not cause problems in the temperature determination. This is because similar spectral shifts will occur for both ro-vibronic molecular transitions [$R(6)$ and $R(7)$] used in this work. The relative vs absolute nature of the temperature measurement leads to a cancellation of factors affecting the slope of the linearized equation for temperature [Eq. (9)]. We have also incorporated a finite laser linewidth in the DIAL modeling. Although this too may affect the S/N ratio, it presents no serious com-

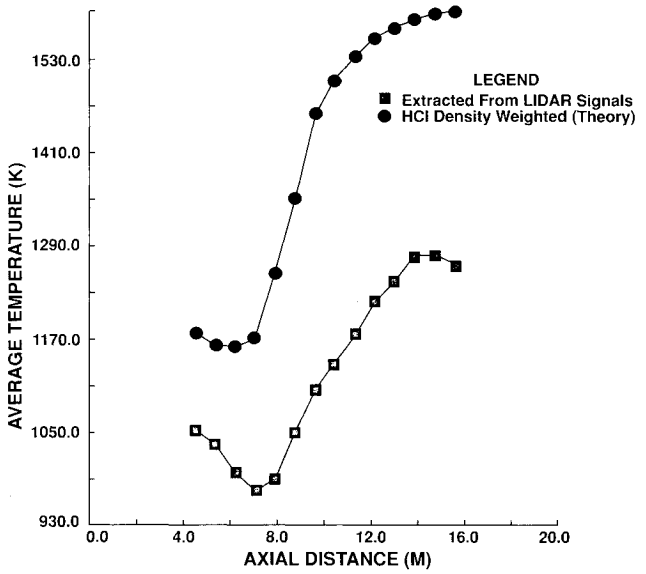

Fig. 8 Average temperatures from DIAL simulation of the Mach disk area, 40-km SPF2 plume, clear atmosphere HCl $R(6)$, $R(7)$ lines, $\Delta X = 1.0\,M$, $\Delta Y = 3.15\,M$, BIN = 1.

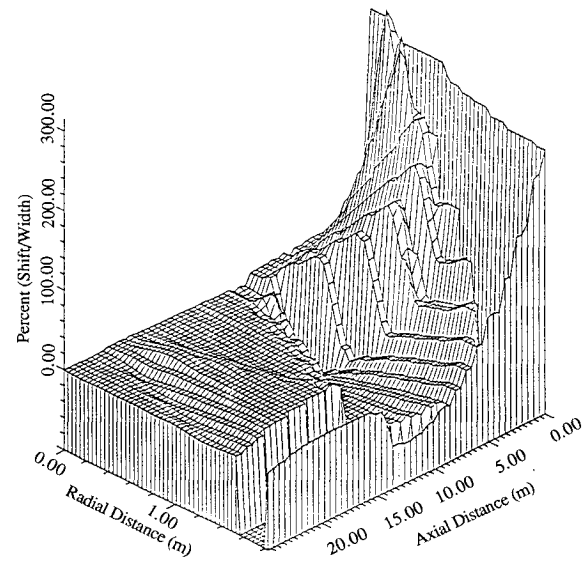

Fig. 10 HCl lineshift/linewidth ratio.

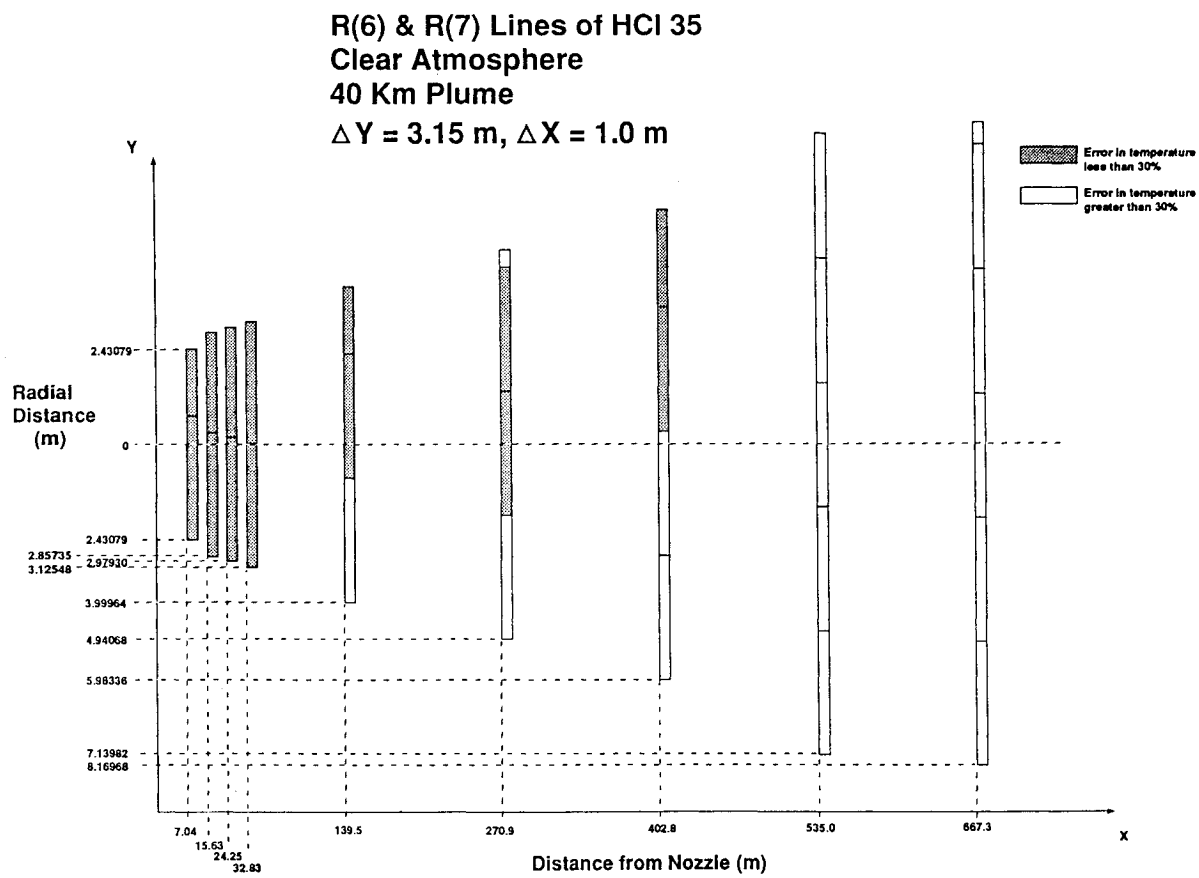

Fig. 9 Predicted error in DIAL temperature measurement.

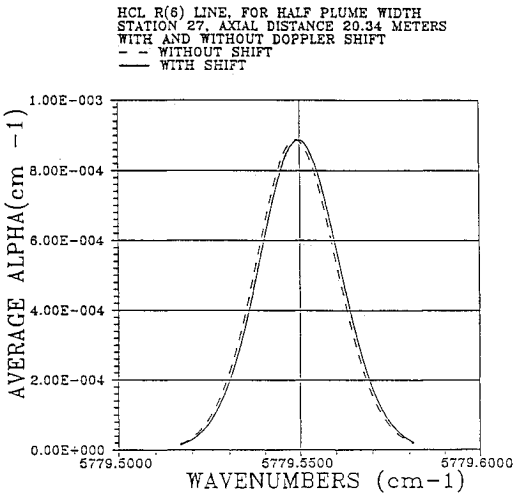

Fig. 11 Doppler shift effect on average absorption coefficient.

plication in the interpretation of the DIAL experimental results.

Conclusions

The numerical simulation presented here has demonstrated that with careful modeling of the expected spatial variability of physical parameters in the plume and atmosphere, the adequacy of proposed DIAL instrumentation and implementation can be evaluated. Important physical effects such as minimum HCl concentration, absorption line shape, hot water and atmospheric interference, and backscatter coefficient wavelength sensitivity have been explored. The SPF2 flowfield solution has been used as a source for prediction of typical HCl and alumina particulate concentrations. The results of the numerical simulation presented here (i.e., the ability to measure a cell averaged temperature for a specified accuracy) should be similar for other flowfield solutions.

The DIAL experiment will, in general, be difficult to conduct because of the need to frequency lock multiple lasers and, for cases like the example of the present study, low HCl plume densities which in turn impose a low error tolerance. Although our results indicate that one may obtain valuable information from a DIAL experiment (such as average gas temperature and location of mach disks), we recommend a stepwise approach to plume diagnostics. A much more practical short term goal would be simple laser backscattering experiments to extract estimates of basic particulate properties and verify the wavelength dependence of β on and off resonance. These preliminary measurements will facilitate the DIAL experiment itself.

References

[1]Christou, C. T., Loda, R. T., Levin, D. A., and Schlinder, A. E., "Simulation of Range Resolved DIAL Measurements on In-Flight Rocket Plumes(U)," Inst. for Defense Analyses, P-2546, DRAFT, Alexandria, VA.

[2]Dash, S. M., Pergament, H. S., Wolf, D. E., and Sinha, H., "The JANNAF Standard Plume Flowfield Model (SPF2)," *11th JANNAF Plume Technology Meeting*, Chemical Propulsion Information Agency, Vol. 1, 1979, pp. 345–442.

[3]Hinkley, E. D., *Laser Monitoring of the Atmosphere*, Topics in Applied Physics, Vol. 14, Springer-Verlag, New York, 1976.

[4]Christou, C. T., and Levin, D. A., "Analysis of Laser Backscattering from Solid Fuel Rocket Plumes," *AIAA Journal*, Vol. 29, No. 8, 1991, pp. 1259–1265.

[5]Brown, B., and McArty, K. P., "Particle Size of Condensed Oxides from Combustion of Metalized Solid Propellants," *8th International Symposium on Combustion*, 1962, pp. 814–822.

[6]Sehgal, R., "An Experimental Investigation of Gas Particle System," Jet Propulsion Lab., TR 32-238, Pasadena, CA, March 1962.

[7]Delaney, I. J., Radke, H. H., and Smith, P., "Exhaust Particle Size Data from Small and Large Solid Rocket Motors," Aerospace Corp., TOR-1001/S2951-18/-3, Los Angeles, CA, July 1967.

[8]Bohren, C. F., and Huffman, D. R., *Absorption and Scattering of Light by Small Particles*, Wiley, New York, 1983.

[9]Walker, J., Malkmus, W., and Ludwig, C. B., "Standardized Infrared Radiation Model (SIRRM)," Vol. 11, Photon Research Associates, Inc., Development and Validation Rept. TR-81-54, La Jolla, CA, Sept. 1981.

[10]Bair, C. H., and Allario, F., "Analysis of Differential Absorption LIDAR Technique for Measurements of Anhydrous Hydrogen Chloride from Solid Rocket Motors Using a Deuterium Fluoride Laser," NASA TN D-8390, May 1977.

[11]Rothman, L. S., et al. "The HITRAN Database: 1986 Edition," *Applied Optics*, Vol. 26, No. 19, 1987, pp. 4058–4097.

[12]Penner, S. S., *Quantitative Molecular Spectroscopy and Gas Emissivities*, Addison-Wesley, Reading, MA, 1959.

[13]Ridgeway, W. L., Moose, R. A., and Cogley, A. C., "Atmospheric Transmittance/Radiance Computer Code FASCOD2," Sonicraft, AFGL-TR-82-0392, Oct. 1982.